地 震 研 究 所 彙 報
Bull. Earthq. Res. Inst.
Univ. Tokyo
Vol. 81 (2006) pp. 341–352

Predicting Strong Ground Motions with a "Recipe"

Kojiro Irikura[1),2)]*

[1)] Kyoto University
[2)] Aichi Institute of Technology

Abstract

A recipe is proposed for estimating strong ground motions from specific earthquakes based on source characteristics from waveform inversion using strong motion data. The main features of the source model are characterized by three kinds of fault parameters, which we call: outer, inner, and extra fault parameters. The outer fault parameters provide overall pictures of the target earthquakes such as entire source area and seismic moment. The inner fault parameters characterize stress heterogeneity inside the fault area. The extra fault parameters are considered to complete the source model, and include starting point and propagation pattern of the rupture. The seismic hazard maps for future large earthquakes with a high probability of occurrence potential are based on the idea of the recipe proposed here by two governmental organizations, the Headquarters of Earthquake Research Center and Central Disaster Prevention Council in Japan.

Key words: strong ground motion, outer fault parameter, inner fault parameter, asperity, effective stress

1. Introduction

From recent developments in waveform inversion analyses for estimating the rupture process using strong motion data during large earthquakes, we have understood that strong ground motions are related to slip heterogeneity inside the source rather than average slip in the entire rupture area. Asperities are characterized as regions that have a large slip relative to the average slip on the rupture area, based on heterogeneous slip distributions that are estimated from source inversion (Somerville *et al.,* 1999). It was found that the asperity areas, as well as entire rupture areas, scale with total seismic moment. Another important study for strong motion prediction showed that strong motion generation areas coincide approximately with asperity areas, where a lot of stress is released (Miyake *et al.,* 2001; Miyake *et al.,* 2003).

Based on the two scaling relationships for the entire rupture area and the asperity areas with respect to the total seismic moment, we found that the source model for predicting strong ground motions is characterized by three kinds of fault parameters: outer, inner, and extra fault parameters. The outer fault parameters are conventional parameters characterizing earthquake size, such as rupture area and seismic moment, and give an overall picture of a source fault. The inner fault parameters are introduced in this study as the combined area of asperities and stress drop of each asperity that define slip heterogeneity inside the source, and which have much more influence on strong ground motions. The extra fault parameters characterize rupture nucleation and termination such as starting point and propagation pattern of the rupture.

So far, most strong motion predictions in earthquake hazard analyses have been made using the empirical attenuation-distance curve for peak ground acceleration (PGA) and peak ground velocity (PGV), in which source information is defined only by seismic magnitude and fault area as outer fault parameters. However, from the source inversion studies mentioned above, we have realized that such parameters are not sufficient to estimate strong ground motions.

We developed a "recipe" for predicting strong

* e-mail: irikura@geor.or.jp (1–8–4, Utsubo-honmachi, Nishi-ku, Osaka, 550–0004, Japan)

ground motions (Irikura and Miyake, 2001; Irikura, 2004), which characterizes the three kinds of fault parameters of source modeling for future large earthquakes. The idea of the "recipe" has been applied in the Seismic Hazard Map for Specified Seismic Source Faults by the Headquarters for Earthquake Research Promotion and the Central Disaster Prevention Council in Japan.

2. Strong Motion Prediction Program in Japan

The basic policy for defining seismic hazard in Japan is based on the 1999 fundamental mission statement governing earthquake research over the next ten years as "The promotion of earthquake research—comprehensive basic policies for the promotion of seismic research through the observation, measurement, and survey of earthquakes," established by the Headquarters for Earthquake Research Promotion (Director: Ministry of Education, Culture, Sports, Science, and Technology). It initiated the creation of seismic hazard maps by promoting surveys of active faults, long-term evaluations of occurrence potential, and predictions of strong ground motions.

Two subcommittees were established under the Headquarters. One is Subcommittee for Long-term Evaluations, which was launched in 1995 to evaluate the probability of earthquake occurrence at active faults and plate boundaries. The other is Subcommittee for Strong Motion Evaluations, which was launched in 1998 to make seismic hazard maps using two different approaches—probabilistic and deterministic.

The probabilistic seismic hazard map is shown as the predicted likelihood of a ground motion level such as PGA, PGV, and seismic intensity occurring in a given area within a set time as shown in Fig. 1. It provides important information for land planning, design standards for structures, and educating people on seismic risks.

The deterministic seismic hazard map is shown as a distribution of ground motion levels predicted for individual specific earthquakes from assumed fault models. The strong ground motions at specific sites near each source fault are estimated as time history, based on the recipe characterizing the source and numerical synthesis of waveforms with a hybrid scheme. Long-period motions are calculated by the

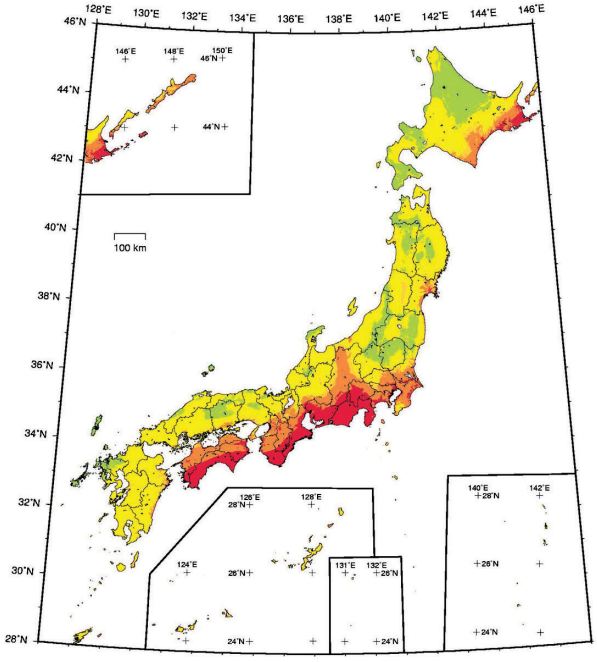

Fig. 1. Probability of suffering strong motions greater than seismic intensity 6- within 30 years from 2005 AD (Earthquake Research Committee, 2005).

finite difference method considering the 3-D structures from source to target sites, and short-period motions are simulated with the stochastic Green's function method (e.g. Irikura and Kamae, 1999). PGA, PGV, seismic intensity, etc., are easily evaluated once the time histories of ground motions are estimated. The time histories of ground motions are useful for nonlinear dynamic analyses of structures, which are needed to design earthquake-resistant buildings and critical structures such as bridges, lifelines, and electric power plants.

The Central Disaster Prevention Council belonging to the Cabinet Office also made deterministic seismic hazard maps for the hypothetical Tokai, Tonankai, and Nankai earthquakes shown as Fig. 2, which are feared likely to occur within the next half century. They made damage and causality estimates to determine disaster management plans for those earthquakes.

3. Scaling Relationships of Fault Parameters

Most of the difficulties predicting strong ground motions involve characterizing source models of future earthquakes. Conventional scaling relations of fault parameters such as fault length and average

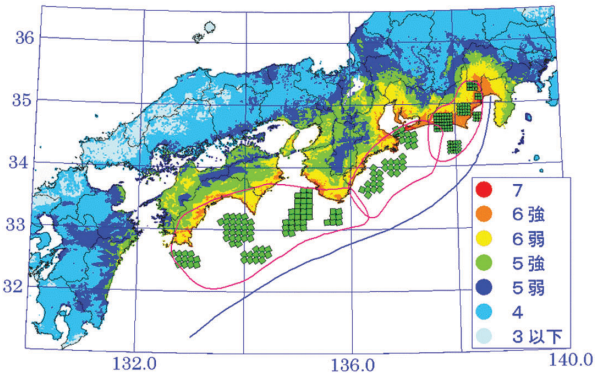

Fig. 2. Seismic intensity map from three hypothetical earthquakes, Tokai, Tonankai, and Nankai earthquakes continuously generated (Central Disaster Prevention Council, 2003).

slip on fault with seismic magnitude are mostly determined geologically from surface offsets and geophysically from forward source modeling using teleseismic data and geodetic data (e.g. Kanamori and Anderson, 1975). Such data are only available for very long period motions, but are not sufficiently available for near-source strong motions dominating short period motions of less than 1 sec of engineering interest. The scaling of fault parameters based on waveform inversion results of the source process using strong motion data gives a clue to solving this problem. We found two scaling relationships—one for the outer fault parameters and the other for the inner fault parameters.

Outer Fault Parameters

The scaling for the outer fault parameters, i.e., relationship between seismic moment and rupture area, for inland crustal earthquakes is summarized in Fig. 3 (a) (Irikura, 2004). For earthquakes with a relatively small seismic moment of less than 10^{19} Nm, the total fault area S seems to follow the self-similar scaling relation with a constant static stress drop in proportion to the two-thirds power of seismic moment M_0. The relation between M_0 and S is given by Eshelby (1957) assuming a circular crack with an average stress drop $\Delta\bar{\sigma}_c$.

$$M_0=\frac{16}{7\pi^{3/2}}\cdot\Delta\bar{\sigma}_c\cdot S^{3/2} \qquad (1)$$

For large earthquakes of more than 10^{19} Nm, scaling tends to depart from the self-similar model (Irikura and Miyake, 2001) corresponding to the saturation of fault width due to seismogenic zone size. Such a two-stage scaling relationship has also been found by Hanks and Bakun (2002). We add one more stage for extra-large earthquakes of more than 10^{21} Nm from the idea of Scholtz (2002), changing L-model to W-model. The scaling relationships in this study shown by broken lines in Fig. 3 (a) assume fault width saturates at a length of 20 km. The relation between M_0 and S for a larger aspect ratio of fault length L of width W is given by Fujii and Matsuura (2000), considering tectonic loading stress.

$$M_0=\frac{\Delta\bar{\sigma}_c W L^2}{aL+b} \qquad (2)$$

For the above equation, a and b are given at 1.4×10^{-2} and 1.0 by Fujii and Matsuura (2000).

Three-stage scaling also seems to be applicable for subduction earthquakes as shown in Fig. 3(b), although the bending points are different. Saturation of fault width for subduction earthquakes becomes longer.

Inner Fault Parameters

Strong ground motions are influenced by inner fault parameters representing slip heterogeneity more than outer fault parameters. The relationships between rupture area S, as the outer fault parameter, and combined area of asperities S_a, as the inner fault parameter, are shown in Fig. 4 (Irikura, 2004). The ratio S_a/S seems to be almost constant regardless of rupture area —about 0.22 for inland earthquake and about 0.25 for subduction earthquake. Then, stress drop on the asperities $\Delta\sigma_a$ is derived as a product of the average stress drop over the fault $\Delta\bar{\sigma}_c$ and the ratio of asperity area S_a to total rupture area S (e.g., Madariaga, 1979).

$$\Delta\sigma_a=\Delta\bar{\sigma}_c\cdot\frac{S}{S_a} \qquad (3)$$

Another empirical relationship between seismic moment M_0 and flat level of acceleration source spectrum A_0 related to inner source parameters is shown in Fig. 5; it was originally found by Dan *et al.* (2001),

$$A_0(dyne\cdot cm/s^2)=2.46\cdot10^{17}\cdot M_0^{1/3}, \qquad (4)$$

where the unit of M_0 is *dyne* · *cm*.

This relation was qualitatively confirmed by other authors (Morikawa and Fujiwara, 2003; Satoh, 2004), although the factor is different depending on

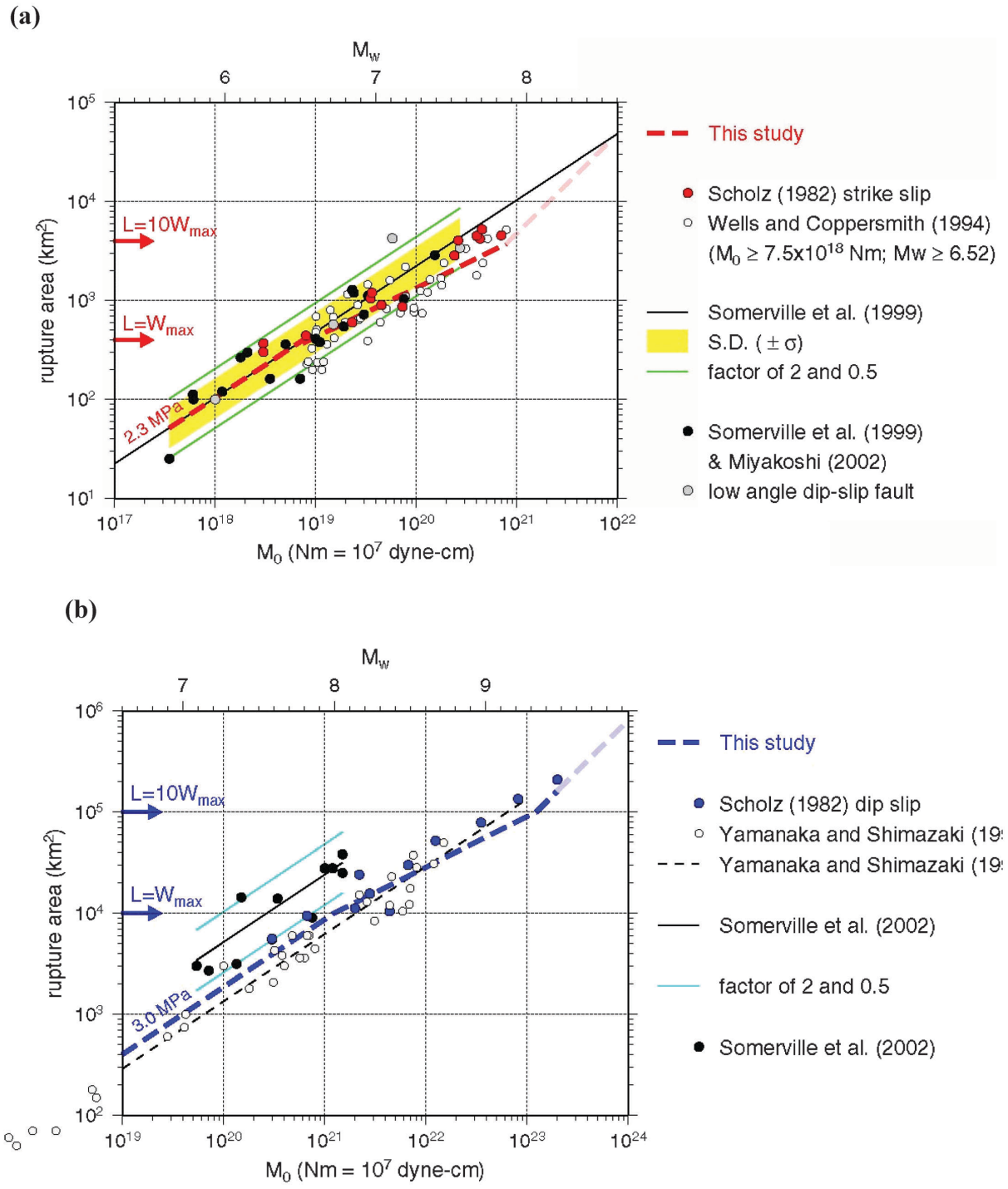

Fig. 3. Empirical relationships between seismic moment and rupture area for inland crustal earthquakes (a) and subduction earthquakes (b). Thick broken lines are 3-stage scaling relationships proposed by our studies (e.g. Irikura, 2004).

earthquake types such as inland-crustal, intra-slab, subduction (interplate) and regionality.

The acceleration source spectral level A_o is obtained by removing propagation-path and surface-geology effects from observed records. A_o is defined as

$$A_0=\sqrt{(A_0^a)^2+(A_0^b)^2},$$

where A_0^a is the acceleration spectral level from asperities and A_0^b is that from background areas.

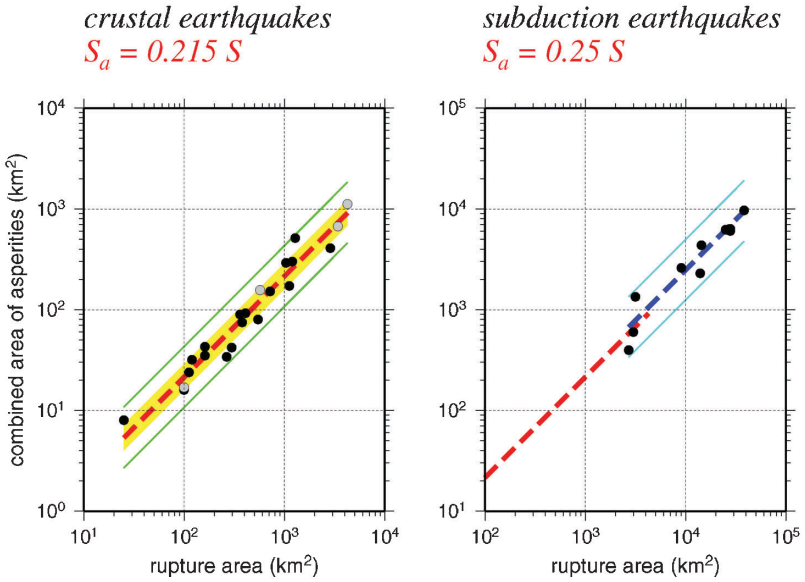

Fig. 4. Empirical relationships between combined area of asperities and total rupture area (thick broken line) for inland crustal earthquakes (left: after Irikura and Miyake, 2001) and subduction earthquakes (right). Shadow ranges $\pm\sigma$ (standard deviation). Thin solid lines show a factor of 2 and 1/2 for the average. Database obtained by the waveform inversions for the inland crustal earthquakes is Somerville *et al.* (1999) and Miyakoshi (2002), for the subduction earthquakes Somerville *et al.* (2002).

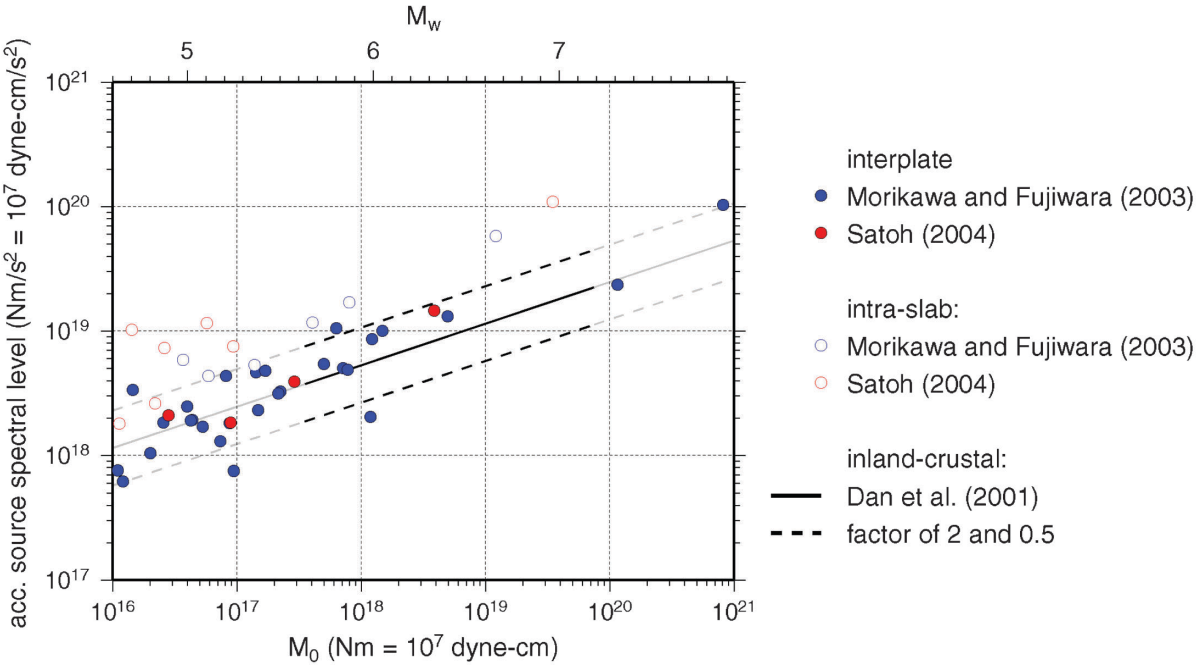

Fig. 5. Empirical relationship between seismic moment and acceleration source spectral level for inland crustal (solid line), intra-slab (open circle) and for subduction (interplate: solid circle) earthquakes.

The acceleration level A_0^a is theoretically proportional to the square root of the combined areas of asperities S_a and the stress drop in the asperities $\Delta\sigma_a$ by Madariaga (1977).

$$A_0^a = 4\sqrt{\pi}\,\beta v_r \Delta\sigma_a \sqrt{S_a}, \tag{5}$$

where β and v_r are S wave velocity of the media and rupture velocity. If A_0^b is relatively small compared to

A_0^a, A_0^a in (5) is replaced by A_0. Then, S_a is estimated as follows.

$$S_a=\left(\frac{7\pi^2}{4}\beta v_r\right)^2 \cdot \frac{(M_0)^2}{S \cdot (A_0)^2} \quad (6)$$

In this case the stress drop of the asperities $\Delta\sigma_a$ is also given as a product of $\Delta\bar{\sigma}_c$ and S/S_a using (3).

4. Recipe for Source Modeling

The procedure for characterizing the source model is outlined as a recipe for estimating three source parameters—outer, inner, and extra fault parameters—as follows:

Estimation of Outer Fault Parameters

Step 1: Total Rupture Area ($S=LW$)

Total fault length L of the specific earthquake is defined as the sum of the lengths of the fault segments grouping simultaneously activated. Fault width W is related to the total fault length before reaching the thickness of the seismogenic zone H_s, and is clipped at $H_s/sin\,\theta$ (θ: dip angle) after reaching there.

$$\begin{aligned} W(\mathrm{km}) &= L \ (\mathrm{km}) && \text{for } L < H_s/sin\theta \\ W(\mathrm{km}) &= H_s/sin\theta \ (\mathrm{km}) && \text{for } L >= H_s/sin\theta \end{aligned} \quad (7)$$

W seems to be clipped at about 20 km when θ is a low angle.

Step 2: Total Seismic Moment (M_0)

The total seismic moment is estimated from the relationship between seismic moment and rupture area (Fig. 3 (a) and (b)).

Step 3: Average Stress Drop ($\Delta\bar{\sigma}_c$) on the Fault

The average static stress-drop for rupture area at the first stage of Fig. 3 ($Mo<10^{19}$ Nm) is estimated by (1) for the circular crack model by Eshelby (1957).

Then, the average stress drop at the second and third stages of Fig. 3 is estimated by (2) for a larger aspect ratio by Fujii and Matsu'ura (2000).

Estimation of Inner Fault Parameters

Step 4. Combined Area of Asperities (S_a)

Two methods are used for the combined area of asperities S_a. One is taken from the empirical relation of S_a versus S (Somerville *et al.* 1999; Irikura and Miyake 2001), where the combined area of asperities is specified to be about 22%. The other is taken from (6), estimating the acceleration source spectral level either from the empirical relation such as (4) or observed records.

Step 5. Stress Drop on Asperities ($\Delta\sigma_a$)

As shown in (3), $\Delta\sigma_a$ as the inner fault parameter is derived as a product of $\Delta\bar{\sigma}_c$ as the outer fault parameter and S_a/S from Step 4.

Step 6. Number of Asperities (N)

The asperities in the entire fault rupture are related to the segmentation of the active faults. Locations of asperities are assumed from various information such as surface offsets measured along faults, back-slip rate studied by GPS observations, and weak reflection coefficients in fault planes.

Step 7: Average Slip on Asperities (D_a)

D_a is given as $2.0 \cdot D$ based on the empirical relationship of Somerville *et al.* (1999). This relationship is approximately confirmed from dynamic simulations of slip distribution with the multiple-asperity source model (Dalguer *et al,* 2004). More precisely, their results show that $D_a/D=2.3$ for $N=1$, $D_a/D=2.0$ for $N=2$, $D_a/D=1.8$ for $N=3$ (N: number of aerities) under constraint Sa/S=0.22 and stress drop of background area $\Delta\sigma_b=0.0$.

Step 8: Effective Stress on Asperity (σ_a) and Background Slip Areas (σ_b)

Effective stress σ_a on asperity for strong motion generation is considered to be identical to stress drop on asperity $\Delta\sigma_a$. Effective stress σ_b on background slip area is constrained by the empirical relationship between seismic moment and acceleration source spectral level.

Step 9: Parameterization of Slip-Velocity Time Functions

The Kostrov-like slip-velocity time functions are assumed as a function of peak slip-velocity and rise time, based on the results of the dynamic simulation of Day (1982). The peak slip-velocity is given as a function of effective stress, rupture velocity, and f_{max}.

Estimation of Extra Fault Parameters

The extra fault parameters are rupture starting point and rupture velocity, which characterize the rupture propagating pattern in the fault plane. For inland crustal earthquakes, rupture nucleation and termination are related to the geomorphology of active faults (e.g., Nakata *et al.*,1998; Kame and Yamashita, 2003). For subduction earthquakes, information from past earthquakes is applied as much as possible.

5. Applicability and Validity of "Recipe"

The "recipe" proposed here has been applied to deterministic seismic-hazard maps for specified seismic source faults with a high probability of occurrence potential in the National Seismic Hazard Maps for Japan (2005). The distribution of ground shaking levels such as PGV and seismic intensity has been evaluated for 10 inland crustal earthquakes and two subduction earthquakes. The availability of the "recipe" has been tested in each application by comparing PGV's of synthesized motions and those derived from the empirical attenuation relationship by Si and Midorikawa (1999).

A more detailed examination has been attempted to show the validity and applicability of the "recipe" comparing simulated ground motions with observed ones for inland crustal earthquakes and subduction earthquakes. We introduce two cases, one is the 1995 Kobe earthquake, as an example of the inland earthquake, and the other is the 2003 Tokachi-oki earthquake, as an example of the subduction earthquake.

1995 Kobe earthquake (Mw 6.9)

The source slip model of the 1995 Kobe earthquake was determined from the inversion of strong ground motion records by several authors (e.g. Sekiguchi *et al.,* 2000 and Yoshida *et al.,* 1996). The slip distributions on the fault plane are similar to each other, although there are clear differences depending on the frequency ranges of the data, smoothing techniques used, etc. Even if the inverted source model is almost uniquely determined, it is not always available for a strong motion simulation. The inversion is usually done using only long-period motions of more than 1 sec.; therefore, it might not be useful for broadband motions including short-period motions of less than 1 sec. of engineering interest.

Then, we refer to the slip model available for broadband ground motions derived from forward modeling using the empirical Green's function method (Kamae and Irikura, 1998). The model consists of three segments: two are at the Kobe side and one is at the Awaji side, as shown in Fig. 6 (a). The outer parameters are given, because the entire rupture area is 51×20.8 km^2, and the total seismic moment is 3.29×10^{23} MPa, assuming $\Delta\bar{\sigma}_c$ to be 2.3 MPa following Steps 1, 2, and 3. Next, the inner fault parameters are given as Sa/S is 0.22, then $\Delta\sigma_a$ is 10.5 MPa. One asperity is distributed in every segment (total of three asperities over the rupture area). The stress drop of the background area is estimated to be about 4.0 MPa from the difference between the stress drop of the asperity directly from Sa/S using (3) and that indirectly from the acceleration level using (5) and (6). Several models are examined to verify the influence of background effective stress σ_b on synthetic motions. Background effective stress σ_b is given as 0.0 MPa for Model 1 and as 4.0 MPa for Model 4. The other parameters are given following Step 4 through Step 9 as summarized in Fig. 6 (b).

Strong ground motions are calculated using the stochastic Green's function method (Kamae *et al.,* 1998). According to this method, the Green's functions are stochastically calculated based on band-limited-white-noise with spectra following the ω^{-2} model, and site effects empirically estimated from observed records of small events. The stochastic Green's functions are changeable depending on the random function in each trial. We choose one representation of those Green's functions whose spectra follow the omega-square model as faithfully as possible.

The synthesized acceleration and velocity motions for Models 1 and 4 are compared with observed motions at KBU very close to the source fault in Fig. 6 (c). The velocity motions show a very good fit between synthesized and observed ones at the right side of Fig. 6 (c), both of which have two significant directivity pulses on two asperities in the forward rupture direction. We find that the most important parameters featuring strong ground motions are sizes of asperities and effective stress on each asperity, which characterizes amplitudes and periods of directivity pulses causing earthquake damage. On the other hand, the synthesized acceleration motions have a larger peak than observed ones at the left side of Fig. 6 (c). There are two possibilities for overestimating acceleration motions. One is that uniform rupture velocity might cause too strong the directivity effect from an asperity near KBU to the synthesized acceleration motions. The other is due to the non-linear behavior of soil layers near the surface. Such high-frequency motions are less effective for evaluating instrumental seismic intensity.

Variability of the synthesized pseudo-velocity response spectra calculated from 10 trials with sto-

(a)

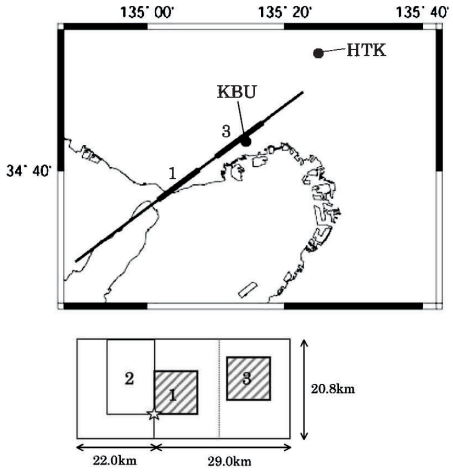

(b)

		M_0 dyne-cm	S km²	D cm	$\Delta\sigma$ MPa	A dyne-cm/sec²
total fault area		3.29×10^{26}	1062	103	2.3	1.70×10^{26}
segment 1	(total)	8.43×10^{25}	300	94	2.3	9.03×10^{25}
	(asperity)	3.57×10^{25}	64	186	10.5	7.29×10^{25}
	(background)	4.86×10^{25}	236	69	4.0	5.33×10^{25}
segment 2	(total)	1.60×10^{26}	462	115	2.3	1.12×10^{26}
	(asperity)	6.96×10^{25}	100	232	10.5	9.12×10^{25}
	(background)	9.04×10^{25}	362	83	4.0	6.50×10^{25}
segment 3	(total)	8.43×10^{25}	300	94	2.3	9.03×10^{25}
	(asperity)	3.57×10^{25}	64	186	10.5	7.29×10^{25}
	(background)	4.86×10^{25}	236	69	4.0	5.33×10^{25}

(c)

(d)

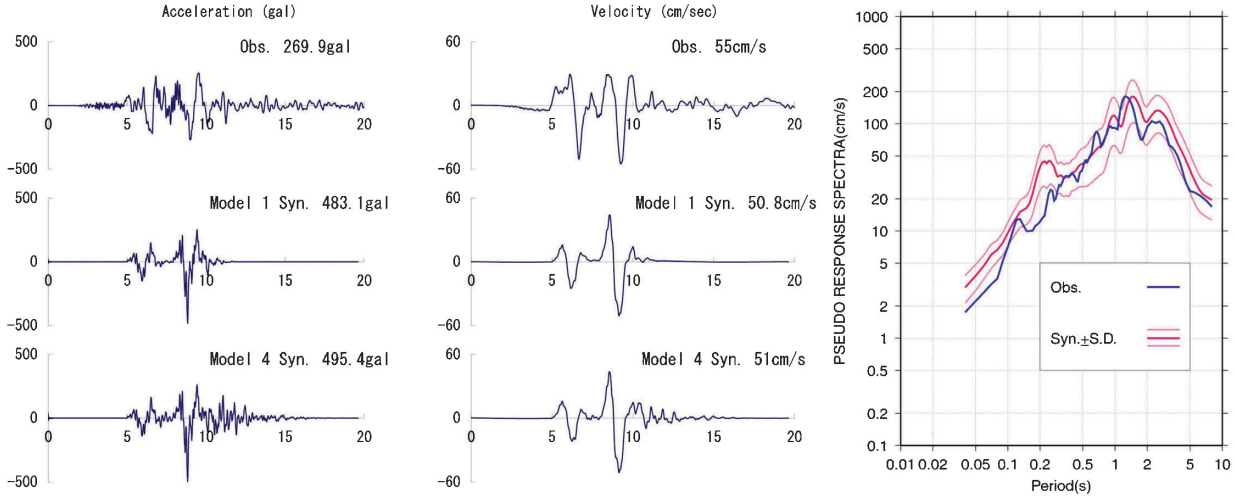

Fig. 6. Ground motion simulation of the 1995 Kobe earthquake using the stochastic Green's function method. (a) Characterized source model based on Kamae and Irikura (1998). (b) Source parameters for synthetic motions. (c) Comparison between observed and synthetic velocities of NS component at KBU station. (d) Variability of synthetic pseudo-velocity response spectra using 10 trials of stochastic Green's functions.

chastic Greens functions is shown for observed ones in Fig. 6 (d). The observed ones range within one standard deviation at periods longer than 0.2 sec, and are effective for measuring seismic intensity. Large deviations of synthesized motions at higher frequencies coincide with overestimation of acceleration motions. We find that strong ground motions from the Kobe earthquake using the "recipe" can be used in practice to predict distributions of seismic intensity.

2003 Tokachi-Oki Earthquake (Mw 8.0)

So far, very few strong motion records for subduction earthquakes have been obtained from around the world. Therefore, we only have less accurate inversion results from slip models of subduction earthquakes. The 2003 Tokachi-oki earthquake provided a large number of strong ground motion records including the source area. Slip models for the earthquake have been proposed by several authors using the waveform inversions of strong motion records (e.g. Honda *et al.*, 2004), teleseismic data (e.g. Yamanaka and Kikuchi, 2003), joint inversions of strong motion and teleseismic data (e.g. Yagi, 2004) and strong motion and geodetic data (Koketsu *et al.*, 2004), and so on.

These results gave us a great opportunity to discuss the validity and applicability of the recipe to subduction earthquakes.

Verification of estimating strong ground motions for this earthquake based on the "recipe" was shown in Report of the National Seismic Hazard Map (2005) by Earthquake Research Committee (2005). We outline the verification mentioned above. The location and geometry of the seismic source fault refer to Honda *et al.* (2004) as shown at the bottom right of Fig. 7. The rupture initiation point is taken at the epicenter determined by the Japan Meteorological Agency.

The order for setting the outer fault parameters is somewhat different from that of the inland earthquakes. The most stable and reliable parameter is seismic moment, which is adopted as $1.05\ 10^{21}$ N-m from the analysis of teleseismic data by Kikuchi and Yamanaka (2003). The rupture area is given to be 9000 km^2, assuming $\Delta\bar{\sigma}_c$ of 3.0 MPa (Kanamori and Anderson, 1975). That is, first *Mo,* second $\Delta\bar{\sigma}_c$ and third *S* are set in order.

The inner fault parameters are given as follows. First, the number of asperities is assumed to be three based on the source inversion results (Yamanaka and Kikuchi, 2003; Honda *et al.,* 2004; Koketsu *et al.,* 2004; Yagi, 2004). The locations of the three asperities are shown by the solid circles inside the source fault in Fig. 7, referring to the result obtained from the forward modeling using the empirical Green's function method of Kamae and Kawabe (2004). The area of the large asperity is 361.2 km^2, and that of the other two asperities is half of the large one. The stress drop of each asperity is estimated at 37.4 MPa from the empirical relation Mo vs acceleration level following Steps 4 and 5. The remaining parameters are given with the "recipe."

The synthesized motions are calculated using a hybrid method (Irikura and Kamae, 1999) with a crossover period of 5 sec, summing up longer period motions with a theoretical procedure and shorter period motions with the stochastic Green's function method. Examples are shown in Fig. 7, in which waveforms and pseudo-velocity-response spectra are compared between observed and synthesized motions at three sites, TKCH11, HDKH05, and HKD093 very near the source fault. We find that the synthesized motions agree well with the observe records.

The instrumental seismic intensity distributions estimated from the observed records and synthesized motions are shown at the left of Fig. 8. Comparison of the seismic intensity between observed records and synthesized motions is shown at the right of Fig. 8. The seismic intensities from the synthesized motions are generally consistent with the observed ones. However, we can see overestimated synthesized motions in some regions where thick sedimentary layers are underlying. This might be due to the empirical formula for estimating instrumental seismic intensity from peak ground velocity. This formula tends to overestimate instrumental seismic intensity with respect to ground motions having a predominant longer than 2 sec.

There still remain many other problems to solve in applying the "recipe" to the subduction earthquake. One of difficulties is to specify the number and locations of asperities when no historical records exist. The other problems arise from difficulties related to a lack of deep basin and off-shore structures from source areas to objective regions, detailed geometries of plate boundaries, etc.

6. Conclusions

A "recipe" for predicting strong ground motions for future large earthquakes is constructed from recent findings of earthquake source physics in seismology and structure damage mechanisms in earthquake engineering. Two scaling relationships are found from the results of the source process by waveform inversion using strong motion data: one is seismic moment M_o versus entire source area S for the outer fault parameters, and the other is M_o versus asperity areas S_a for the inner fault parameters.

The source model is defined by three kinds of fault parameters: outer, inner, and extra fault parameters following the "recipe" based on the scaling relationships. In this study the validity and applicability of the procedures for characterizing earthquake sources based on the "recipe" are examined in comparison with observed records and broad-band simulated motions for the 1995 Kobe and the 2003 Tokachi-oki earthquakes.

The synthesized ground motions following the "recipe" for the 1995 Kobe earthquake are consistent with observed records of velocity and seismic intensity, but overestimate acceleration at a very near

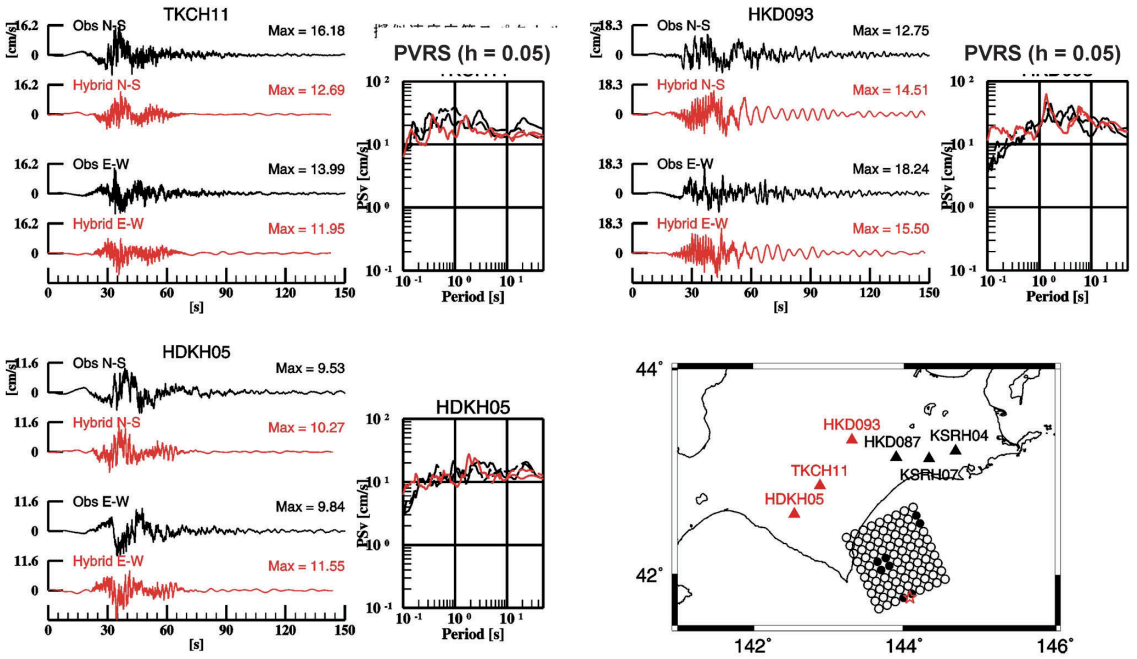

Fig. 7. Comparison of waveforms and pseudo-velocity-response spectra (PVRS, h=0.05) between those observed and synthesized from the 2003 Tokachi-oki earthquake. Map showing source model and observation stations is at the right bottom.

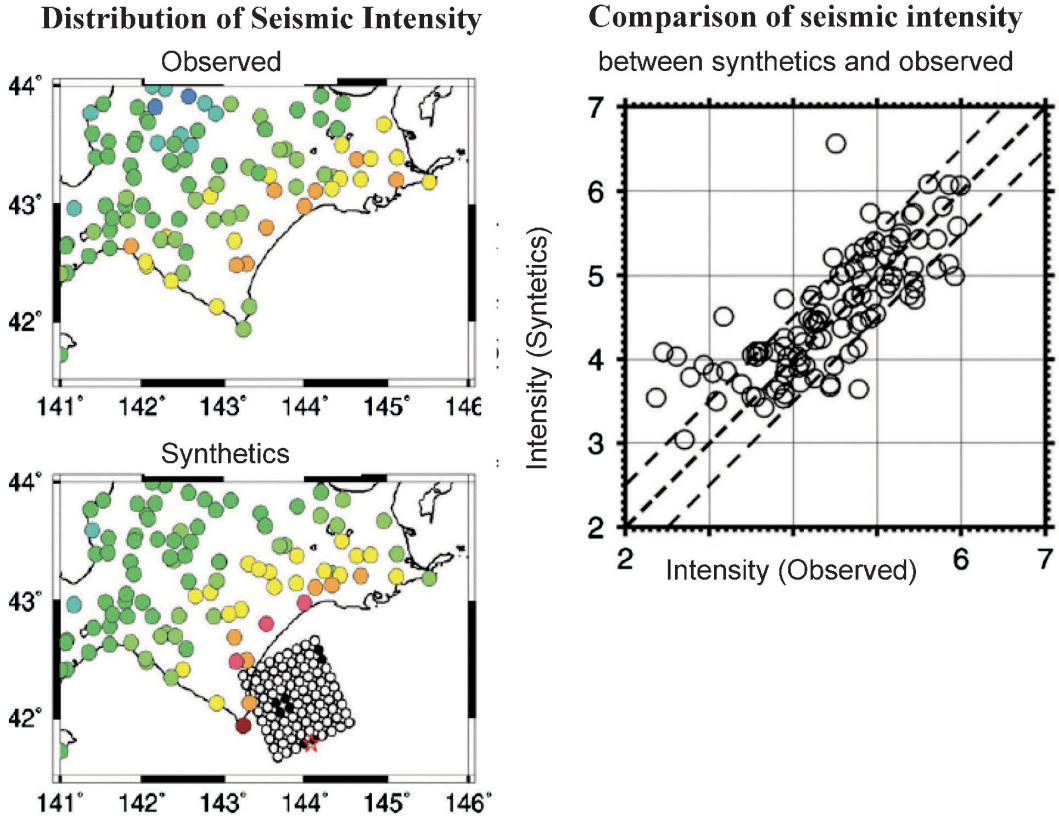

Fig. 8. Comparison of seismic intensity between observed and synthetics for the 2003 Tokachi-oki earthquake. Left: distribution of seismic-intensity from observed records (Upper map) and synthetic motions (Lower map). Left lower: comparison of seismic intensity between synthetics and observed.

station. The most important parameters featuring strong ground motions are sizes of asperities and effective stress on each asperity, which characterize the amplitudes and periods of directivity pulses causing earthquake damage.

The ground motions for the 2003 Tokachi-oki earthquake, as an example of a subduction earthquake, are successfully simulated based on the "recipe," showing good agreement in the spatial pattern of seismic intensity, as well as in the waveform between observed and synthetics. However, we need a priori information for specifying the number of asperities and their locations, as well as the location and geometry of the source fault. It is very difficult to specify such source parameters when no historical records exist.

Acknowledgments

This study was done as a part of the governmental project of "National Seismic Hazard Map in Japan" sponsored by the Headquarters for Earthquake Research Promotion of Japan under the Ministry of Education, Culture, Sports, Science, and Technology. I express deep thanks for allowing me to refer to the results and figures of the Seismic Hazard Map presented by the Earthquake Research Committee. I am grateful to Hiroe Miyake and Katsuhiro Kamae for their contributions to this study.

References

Central Disaster Prevention Research Institute, 2003, Estimated Seismic Intensity Distribution in the case of Simultaneous Occurrence of Three Earthquakes, Tokai, Tonankai, and Nankai, 16th Special Survey Committee of Tonankai and Nankai earthquake, http://www.bousai.go.jp/jishin /chubou/nankai/16/index.html (in Japanese).

Dalguer, L.A., H. Miyake, K. Irikura, 2004, Characterization of dynamic asperity source models for simulating strong ground motions, *Proceedings of the 13th World Conference on Earthquake Engineering,* No.3286, CD-ROM.

Dan K, Watanabe T, Sato T, Ishii T., 2001, Short-period source spectra inferred from variable-slip rupture models and modeling of earthquake fault for strong motion prediction, *Journal of Struct. Constr. Engng. AIJ,* **545**, 51–62.

Das S and B.V. Kostrov, 1986, Fracture of a single asperity on a finite fault, *Earthquake Source Mechanics, Geophysical Monograph 37, Maurice Ewing Series* **6**, *American Geophysical Union,* 91–96.

Day, S.M., 1982, Three-dimensional simulation of spontaneous rupture: the effect of nonuniform prestress, *Bull. Seism. Soc. Am.,* **88**, 512–522.

Earthquake Research Committee, 2005, National Seismic Hazard Map for Japan (2005), *Report published by the Headquarters of Earthquake Research Promotion under the Ministry of Education, Culture, Sports, Science, and Technology,* 121p. (in Japanese).

Earthquake Research Committee, 2005, 4.3.13 Verification results using observed records of the 2003 Tokachi-Oki Earthquake, *National Seismic Hazard Map for Japan (2005),* http://www.jishin.go.jp/main/index-e.html

Eshelby J.D., 1957, The determination of the elastic field of an ellipsoidal inclusion, and related problems," *Proc.. Roy Soc.,* **A241**, 376–396.

Fujii, Y. and M. Matsu'ura, 2000, Regional difference in scaling laws for large earthquakes and its tectonic implication, *PAGEOPH,* **157**, 2283–2302.

Hanks, T.C. and W.H. Bakun, 2002, A bilinear source-scaling model for M-logA observations of continental earthquakes, *Bull. Seism. Soc. Am,* **92,** 1841–1846.

Honda, R., S. Aoi, N. Morikawa, H. Sekiguchi, K. Kunugi and H. Fujiwara, 2004, Ground motion and rupture process of the 2003 Tokachi-oki earthquake obtained from strong motion data of the K-NET and KiK-net, *Earth Planets and Space* **56**, 317–322.

Irikura K., 2004, Recipe for predicting strong ground motion from future large earthquake, *Annuals of Disaster Prevention Research Institute,* **47A**, 25–45 (in Japanese).

Irikura K and K. Kamae, 1999, Strong ground motions during the 1948 Fukui earthquake, *Zisin,* **52**, 129–150 (in Japanese).

Irikura K. and H. Miyake H., 2001, Prediction of strong ground motions for scenario earthquakes, *Journal of Geography,* **110**, 849–875 (in Japanese with English abstract).

Kame N. and T. Yamashita T., 2003, Dynamic branching, arresting of rupture and the seismic wave radiation in self-chosen crack path modeling, *Geophys. J. Int.,* **155**, 1042–1050.

Kamae K. and K. Irikura, 1998, Rupture process of the 1995 Hyogo-ken Nanbu earthquake and simulation of near-source ground motion, *Bull. Seism. Soc. Am.,* **88**, 400–412.

Kamae, K., K. Irikura and A. Pitarka, 1998, A technique for simulating strong ground motion using hybrid Green's function, *Bull. Seism. Soc. Am.,* 88, 357–367.

Kamae, K. and H. Kawabe, 2004, Source model composed of asperities for the 2003 Tokachi-oki, Japan, earthquake (M_{JMA}=8.0) estimated by the empirical Green's function method, *Earth Planets and Space* **56**, 323–327.

Kanamori H. and D.L. Anderson, 1975, Theoretical basis of some empirical relations in seismology, *Bull. Seism. Soc. Am.,* **86**, 1073–1095.

Kikuchi M. and Y. Yamanaka, 2001, Rupture processes of past large earthquakes=Identification of asperities, *Seismo,* **5**, 6–7.

Koketsu, K., K. Hikima, S. Miyazaki and S. Ide, 2004, Joint inversion of strong motion and geodetic data for the source rupture process of the 2003 Tokachi-oki, Hokkaido, earthquake, *Earth Planets and Space* **56**, 329–334.

Madariaga, R., 1977, High frequency radiation from crack (stress drop) models of earthquake faulting, *Geophys. J. R. Astron. Soc.,* **51**, 625–651.

Madariaga, R., 1979, On the relation between seismic moment and stress drop in the presence of stress and strength heterogeneity, *J. Geophys. Res.,* **84**, 2243–2250.

Miyake, H., T. Iwata and K. Irikura, 2001, Estimation of rupture propagation direction and strong motion generation area from azimuth and distance dependence of source amplitude spectra, *Geophys. Res. Lett.,* **28**, 2727–2730.

Miyake H, T. Iwata, K. Irikura, 2003, Source characterization for broadband ground motion simulation: Kinematic heterogeneous source model and strong motion generation area, *Bull. Seism. Soc. Am.,* **93**, 2531–2545.

Miyakoshi, K., T. Kagawa, H. Sekiguchi, T. Iwata and K. Irikura, 2000, Source characterization of inland earthquakes in Japan using source inversion results, *Proc. 12 th World Conf. Earthq. Eng.* (CD-ROM).

Morikawa N. and H. Fujiwara, 2003, Source and path characteristics for off Tokachi-Nemuro earthquakes, *Programme and Abstracts for the Seismological Society of Japan, 2003 Fall Meeting,* 104 (in Japanese).

Nakata T, Shimazaki K, Suzuki Y, Tsukuda E., 1998, Fault branching and directivity of rupture propagation, *Journal of Geography,* **107**, 512–528 (in Japanese).

Satoh T., 2004, Short-period spectral level of intraplate and interplate earthquakes occurring off Miyagi prefecture, *Journal of JAEE'2004,* **4**, 1–4 (in Japanese with English abstract).

Scholz, C.H., 1982, Scaling laws for large earthquakes: Consequences for physical models, *Bull. Seism. Soc. Am.,* **72**, 1–14.

Scholz C.H., 2002, The mechanics of earthquakes and faulting, *Cambridge University Press.*

Sekiguchi, H., Irikura, K. and Iwata, T., 2000, Fault geometry at the rupture termination of the 1995 Hyogo-ken Nanbu earthquake, *Bull. Seism. Soc. Am.,* **90**, 974–1002.

Si, H. and S. Midorikawa, 1999, New attenuation relationships for peak ground acceleration and velocity considering effects of fault type and site condition, *J. Struct. Constr. Eng., AIJ,* **523**, 63–70 (in Japanese with English abstract).

Somerville P, K. Irikura, R. Graves, S. Sawada, D. Wald, N. Abrahamson, Y. Iwasaki, T. Kagawa, N. Smith, A. Kowada, 1999, Characterizing earthquake slip models for the prediction of strong ground motion, *Seism. Res. Lett.,* **70**, 59–80.

Somerville, P.G., T. Sato, T. Ishii, N.F. Collins, K. Dan and H. Fujiwara, 2002, Characterizing heterogeneous slip models for large subduction earthquakes for strong ground motion prediction. *Proc. 11th Japan Earthquake Symposium.*

Wells, D.L. and K.J. Coppersmith (1994): New empirical relationships among magnitude, rupture length, rupture width, rupture area, and surface displacement, *Bull. Seism. Soc. Am.,* Vol. 84, pp. 974–1002.

Yagi, Y., 2004, Source rupture process of the 2003 Tokachi-oki earthquake determined by joint inversion of teleseismic body wave and strong ground motion data, *Earth Planets and Space* **56**, 311–316.

Yamanaka Y, M. Kikuchi M, 2003, Source process of the recurrent Tokachi-oki earthquake on September 26, 2003, inferred from teleseismic body waves, *Earth Planets Space,* **55**, e21–e24.

Yoshida, S., K. Koketsu, B. Shibazaki, T. Sagiya, T. Katoand Y. Yoshida, 1996, Joint inversion of the near- and far-field waveforms and geodetic data for the rupture process of the 1995 Kobe earthquake, *J. Phys. Earth,* **44**, 437–454, 1996.

(Received September 14, 2006)
(Accepted February 24, 2007)